



Seasonal changes in metal and nutrient fluxes across the sediment-water interface in tropical mangrove creeks in the Amazon region

Christiene R.L. Matos^{a,*}, José F. Berrêdo^a, Wilson Machado^b, Edouard Metzger^c, Christian J. Sanders^d, Kelson C.F. Faial^e, Marcelo C.L. Cohen^f

^a Museu Paraense Emílio Goeldi/MCTIC, Belém, Pará, Brazil

^b Programa de Pós-Graduação em Geoquímica, Universidade Federal Fluminense, Niterói, Rio de Janeiro, Brazil

^c Laboratoire de Planétologie et Géosciences, CNRS, Université d'Angers, Nantes Université, Le Mans Université, Angers, France

^d National Marine Science Centre, Southern Cross University, Coffs Harbour, New South Wales, Australia

^e Laboratório de Toxicologia, Seção de Meio Ambiente, Instituto Evandro Chagas, Belém, Pará, Brazil

^f Programa de Pós-Graduação em Geologia e Geoquímica, Universidade Federal do Pará, Belém, Pará, Brazil

ARTICLE INFO

Editorial handling by Michael Kersten

Keywords:

Seasonal variations
Intertidal environmental
Organic matter degradation
Pore water exchange
Sediment-water interface

ABSTRACT

Mangrove creeks are considered important routes between terrestrial and adjacent coastal waters regarding the transport of dissolved material to oceans. The present study assessed if Amazonian seasonal rainfall patterns affect the pore water biogeochemistry and the intensity and direction of nutrient (NH_4^+ and PO_4^{3-}) and metal (Fe^{2+} and Mn^{2+}) exchanges from intertidal creek mudflats fringed by pristine mangroves. The results indicate that mangrove-fringed mudflats are effective in retaining iron and nutrients in solid sediment phases compared to export to coastal waters, also potentially comprising a significant manganese contributor to coastal waters. However, nutrient and metal retention are lower during the wet season, as intense rainfall periods reduce pore water salinity and promote increased reducing sediment conditions. Such conditions enhance organic matter degradation and pore water NH_4^+ , PO_4^{3-} , Fe^{2+} and Mn^{2+} concentrations just below the sediment-water interface, generating higher effluxes during this period. Our findings demonstrate that seasonal variabilities drive substantial physicochemical property and pore water biogeochemistry changes, affecting the efficiency of mudflat sediments retaining and exporting nutrients and metals.

1. Introduction

Mangroves occur along the land-ocean interface under the influence of both fresh and seawater. These ecosystems, whether pristine or disturbed, can act as sinks and store significant amounts of carbon (Alongi, 2020a), nutrients (Breithaupt et al., 2014; Sanders et al., 2014) and metals (Marchand et al., 2011; Thanh-Nho et al., 2019) in their sediments. Alternatively, mangroves may also play an essential role in exchanging of dissolved and particulate matter between terrestrial and oceanic environments (Dittmar et al., 2006; Jennerjahn and Ittekkot, 2002). The capacity of mangrove systems to act as net sinks or sources of nutrient and metal is influenced by many factors, including the input of terrestrial or oceanic nutrients, shifts in redox conditions, anthropogenic activities, and local environmental factors such as weather conditions, hydrology, tidal range, latitude, mangrove community structure and

topographic elevation (Adame et al., 2010; Adame and Lovelock, 2011; Kristensen et al., 2017).

Mangrove creeks are considered important routes between forest environments and adjacent coastal waters regarding the transport of dissolved and suspended materials (Dittmar and Lara, 2001; Lacerda et al., 1999). However, mangrove sediment creeks also can act as biogeochemical reactors, and their pore water can become a crucial source of dissolved metals and nutrients to coastal areas, if these elements are not efficiently removed from pore waters by precipitation and sorption processes in the upper sediment layers (Ogrinc and Faganeli, 2006; Rozan et al., 2002). The exchange of dissolved elements can take place essentially by spontaneous molecular diffusion across the sediment-water interface (SWI) including in macrotidal regimes (Alongi et al., 2004; Bally et al., 2004; Pan et al., 2020; Pratihary et al., 2021; Thibault de Chanvalon et al., 2017; Wang et al., 2011), through pore

* Corresponding author. at: Museu Paraense Emílio Goeldi, Av. Perimetral, 1901 – CEP. 66077-830, Belém, Pará, Brazil .

E-mail addresses: christienematos@hotmail.com (C.R.L. Matos), berredo@museu-goeldi.br (J.F. Berrêdo), wmachado@geoq.uff.br (W. Machado), edouard.metzger@univ-angers.fr (E. Metzger), christian.sanders@scu.edu.au (C.J. Sanders), kelsonfaial@iec.gov.br (K.C.F. Faial), mcohen80@hotmail.com (M.C.L. Cohen).

<https://doi.org/10.1016/j.apgeochem.2022.105217>

Received 17 August 2021; Received in revised form 21 January 2022; Accepted 22 January 2022

Available online 25 January 2022

0883-2927/© 2022 Elsevier Ltd. All rights reserved.

water seepage into tidal creek water columns during low and ebbing tides (Holloway et al., 2016; Sanders et al., 2015; Taillardat et al., 2019; Tait et al., 2017) or transported by bioturbation (irrigation from burrows and biodiffusion) (Bouillon et al., 2007; Ovalle et al., 1990).

In addition to tides, regional seasonality also influences estuarine water quality. Mangroves developed under the Amazon hydrological regime, for example, are subject to high annual rainfall rates which, in turn, lead to high seasonal freshwater inputs and fluvial water discharges, causing extreme salinity fluctuations within estuaries and tidal

creeks. Therefore, the biogeochemistry of these waters alter at both the temporal (seasonal, tidal, diel) and spatial scales, due to seasonal fluvial discharge and organic matter (OM) input from different sources (mainly mangroves and phytoplankton). Previous assessments have reported that the documented seasonal rainfall patterns can lead to seasonal changes in sedimentary physical and chemical properties (Alongi et al., 2004; Berrêdo et al., 2016; Marchand et al., 2004) pore water chemistry (Lee et al., 2008; Taillardat et al., 2019; Thanh-Nho et al., 2020; Wu et al., 2015) and nutrient and metals fluxes to coastal waters (Adame

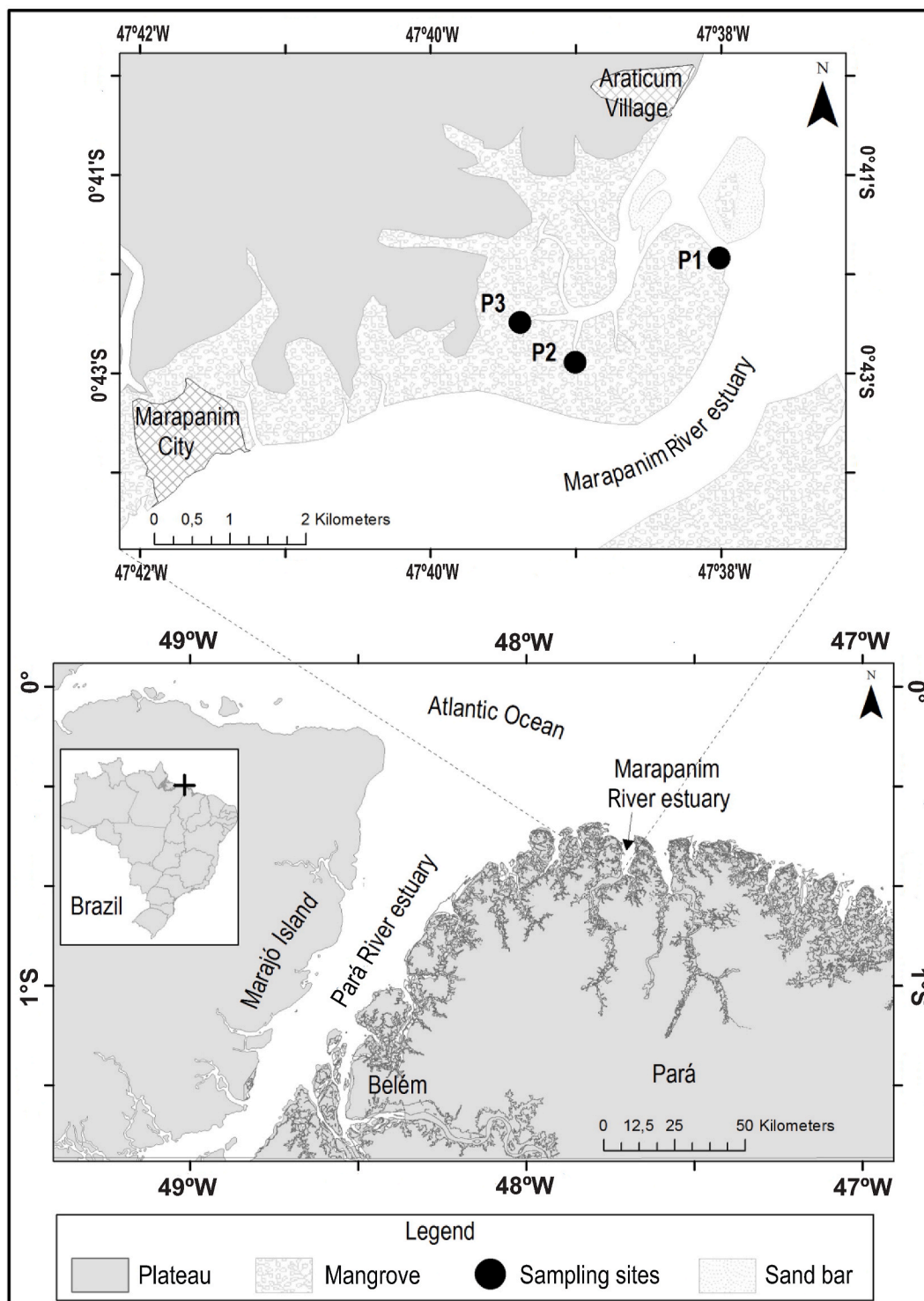


Fig. 1. Map displaying the Marapanim estuary study area, in the state of Pará, Brazil, indicating the P1, P2 and P3 sampling sites.

et al., 2010; Alongi et al., 2001; Rao et al., 2018; Yasui et al., 2016). Therefore, local weather conditions in the estimation and management of nutrient and metal budgets, especially in small mangrove rivers (Terada et al., 2017), must be considered.

In the present study, Amazonian seasonal rainfall patterns are hypothesized to significantly affect the physicochemical properties and pore water biogeochemistry of creek mudflats, as well as metal and nutrient fluxes at the SWI. To assess rainfall effects on creek mudflats sediment and pore water dynamics, field observations were conducted in three intertidal mudflat sediments fringed by pristine mangroves in the Marapanim River Estuary (MRE), northern Brazil, in both the wet (April 2017) and dry (September 2017) seasons. To this end, the temporal and spatial distributions of pH, Eh, salinity, Cl^- , SO_4^{2-} , Fe^{2+} , Mn^{2+} , total alkalinity (TA) and nutrients (NH_4^+ and PO_4^{3-}) were first obtained alongside sediment parameters. Diffusive nutrient and metal fluxes between sediment pore waters and the overlying water were subsequently estimated. Finally, rainfall effects on the physicochemical conditions, pore water biogeochemistry and nutrient and metal fluxes at the SWI, and the importance of the creek mudflats to coastal biogeochemical cycles were then assessed.

2. Materials and methods

2.1. Study area

The MRE, located in the state of Pará, northern Brazil (00°30' to 01°00'S and 47°32' to 47°00'W, Fig. 1), can be subdivided into three morphologic realms, namely the coastal, estuarine and alluvial plains (Silva et al., 2009). The sedimentary deposits of the Coastal Plateau are represented by cliffs and lateritic soils (Pleistocene) derived from the Barreiras Formation (Tertiary), the main source of sand, silt and clay fractions, comprising quartz, clay minerals (kaolinite and illite), iron oxides, and recent sediments (Holocene) that constitute mangrove substrates (Berrêdo et al., 2008a). The estuarine plain where mangroves are established presents sandy and muddy deposits (Silva et al., 2009).

The tidal flats of the MRE are occupied by well-developed mangroves, which are part of the largest continuous and best-preserved mangrove forest in the world (Kauffman et al., 2018; Nascimento et al., 2013). The main river channel is about 70 and 8 km long and wide at the mouth, presenting the incursion of oceanic waves from Atlantic and semi-diurnal macrotides that present a tidal range of 3.5 m during neap tides and over 6 m during spring tides (Silva et al., 2009). Saline waters penetrate approximately 62 km up the main river channel during the dry season and 42 km during the wet season (Berrêdo et al., 2008b).

The coastal region of Pará is characterized by a tropical climate with two distinct seasons. The wet season occurs between January and June, when total rainfall often exceeds 2000 mm, with a mean April rainfall of 462 mm. The dry season ranges from July to December, with a mean September rainfall of 5 mm. The annual mean temperature is 27.7 °C. The estuary water temperature ranges from 27 to 30 °C. The pH values along the estuarine channel range between alkaline (7.9–8.0) to slightly acidic (5.7–6.7) during the dry and wet seasons, respectively (Berrêdo et al., 2008b).

The samplings were carried out along three intertidal mudflats, numbered according to their distance from the main Marapanim River, with number 1 (P1) comprising the Marapanim River margin, and number 2 (P2) and 3 (P3) located at two tidal mangrove creeks along the Marapanim mangrove forest (Fig. 1). Sites P1 and P2 are 2.3 km apart, while site P3 is located ~1 km from P2. The tidal creeks do not receive any direct freshwater inputs except for rainwater and runoff from the Marapanim River during the wet season. They exhibit sinuous bifurcated forms, are shallow (3 m in depth), about 5 km long and 800 m wide, and are under the influence of the semidiurnal tide regime, with 6 h intervals between the ebb and flood tides. The three sampling sites are frequently exposed during the low tide.

2.2. Solid-phase sediment sampling and analyses

To assess the effects of contrasting seasons, two replicate cores were collected from the intertidal mudflat at each site, during the wet (April 2017) and dry (September 2017) seasons. Acrylic tubes (50 cm length, 8 cm diameter) were used to recover approximately 35 cm of sediment and 15 cm of overlying water at a water column depth of ~0.8 m. One core, dedicated to solid-phase analyses, was sliced at 1-cm (0–6 cm), 2-cm (6–20 cm), and 5-cm intervals (20–35 cm depth). The sub-samples were stored in polyethylene bags at 4 °C until processing. An aliquot of humid sediment was fixed with Zn-acetate, within a N_2 -filled glove bag, for the determinations of acid volatile sulfides (AVS, mainly Fe monosulfide/FeS) and chromium reducible sulfur (CRS, mainly pyrite/FeS₂).

The most reactive Fe (Fe_R) and Mn (Mn_R) fractions were determined using the ascorbate reagent (50 g NaHCO_3 , 50 g Na-citrate, 20 g ascorbic acid to a 1 L solution, buffered at pH 8) (Anschutz et al., 2005; Kostka and Luther, 1994). Extractions were carried out using 500 mg of dried sediment in 10 mL of N_2 -degassed ascorbate reagent for 24 h under continuous shaking. The supernatant was diluted 10-fold with HNO_3 (1.0%), and Fe and Mn concentrations were determined by atomic absorption spectrometry using an external standard prepared in the same matrix. Total organic carbon (TOC) depth profiles were obtained from Matos et al. (2020). AVS and CRS were determined in 1 g of sediment by a two-step distillation with cold 6 N HCl followed by boiling 2 N acidic CrCl_2 solution (Fossing and Jørgensen, 1989). The liberated H_2S was collected in Zn-acetate (20%) traps, and its concentration was determined according to the method of Cline (1969).

2.3. Pore water sampling and analyses

Regarding the second replicate core, pH and redox potential (Eh) were measured with a pH meter electrode (Metrohm 826 pH mobile) directly in the sediment through holes in one specific predrilled tube, in the same intervals as in the solid-phase, which were covered with tape during the sampling. After determining the redox-pH, following the same intervals, the overlying and pore waters were removed using Rhyzon® collectors (7 cm and 0.1 μm in length and pore diameter, respectively), inserted directly into the sediment through pre-drilled holes along the acrylic tubes (Seeborg-Elverfeldt et al., 2005). The overlying water sampling comprised ~5 cm above the SWI.

The pore water samples were treated in a N_2 -filled glove bag to prevent oxidation. The overlying and pore water samples were analyzed concerning Cl^- , SO_4^{2-} , Fe^{2+} , Mn^{2+} , total alkalinity (TA), NH_4^+ and PO_4^{3-} and total dissolved sulfide ($\Sigma\text{H}_2\text{S} = \text{H}_2\text{S} + \text{HS}^- + \text{S}_0 + \text{S}_x^{-2}$). A total of 2 mL of water samples were deposited in amber vials for the alkalinity analyses. Subsamples (1 mL) were preserved in Eppendorf tubes using 100 μL of a 5% Zn-acetate solution and 10 μL HCl for the $\Sigma\text{H}_2\text{S}$ and PO_4^{3-} analyses, respectively. Samples (1 mL) were preserved in Eppendorf tubes for the SO_4^{2-} and Cl^- analyses. All samples were maintained at 4 °C. Other sub-samples (1 mL) were frozen in amber vials for subsequent NH_4^+ analyses.

Dissolved Fe and Mn concentrations were determined employing an ICP-OES (VISTA-MPX CCD Simultaneous) using 10-fold dilutions. Accuracies were checked using a natural water reference NIST (1640a, 1643e), and were within 5% for Fe and Mn. TA was determined through potentiometric Gran titration using 0.01 mol L⁻¹ HCl immediately after vial removal from the glove-bag. Standard colorimetric methods were used to determine the NH_4^+ and PO_4^{3-} concentrations (Gieskes et al., 1991). $\Sigma\text{H}_2\text{S}$ concentrations were quantified through the colorimetric method as proposed by Cline (1969). The SO_4^{2-} and Cl^- concentrations of were measured by ion chromatography (Dionex DX 120) applying a 500-fold dilution. Salinity was determined using a portable refractometer (Atago).

2.4. Sulfate depletion calculation

Chloride is a conservative element, as it is not affected by biological or chemical processes. It was therefore, employed to evaluate sulfate depletion ($SO_4^{2-}_{Dep}$) under freshwater dilution and microbial removal effects. Sulfate concentrations were normalized according to chloride concentration changes, according to Eq. (1):

$$(SO_4^{2-})_{Dep} = [(Cl^-)_{pw} \cdot (R_{sw})^{-1}] - (SO_4^{2-})_{pw} \quad (1)$$

where $(SO_4^{2-})_{Dep}$ comprised SO_4^{2-} depletion, $(Cl^-)_{pw}$ and $(SO_4^{2-})_{pw}$ consists in the pore water concentrations of Cl^- and SO_4^{2-} , and R_{sw} is the molar ratio of Cl^- to SO_4^{2-} in surface seawater ($R_{sw} = 19.33$; Weston et al., 2006). Sulfate depletion reveals the net consumption of microbially mediated of SO_4^{2-} (Weston et al., 2006).

2.5. Metal and nutrient flux estimations

The diffusive metal and nutrient flux estimates between sediment pore waters and the overlying water were calculated from the interfacial concentration gradients, according to Fick's first law of diffusion (Berner, 1980) below:

$$F = -\phi D_s (\Delta C / \Delta Z) \quad (2)$$

where F ($mmol \cdot m^{-2} \cdot d^{-1}$) is the diffusive flux, ϕ (dimensionless) is the porosity at the sediment surface (depth = 0–1 cm), D_s ($m^2 \cdot s^{-1}$) is the molecular diffusion coefficient in sediment, and $\Delta C / \Delta Z$ comprises the concentration gradient across the SWI. According to these calculations, negative fluxes reflect sediment uptake processes (i.e., downward fluxes), whereas positive fluxes indicate benthic recycling (i.e., outward fluxes to overlying waters). Porosity was expressed and calculated as the water volume fraction in the wet sediment, which was identified by the weight difference between wet sediment samples before and after drying at 60 °C. $\Delta C / \Delta Z$ consists in the concentration gradient in the overlying water and pore water. The diffusion coefficient (D_s) was calculated from the molecular diffusion coefficient in free water D_0 corrected for sediment porosity and temperature (Li and Gregory, 1974). The upper sediment layers presented porosities between 0.51 and 0.76, and overlying waters ranged between 28.0 and 29.3 °C.

2.6. Statistical analyses

Statistical assessments were carried out using the statistical package PAST version 3.26 (Hammer et al., 2001). Potential differences regarding dissolved and solid-phase concentrations between the sampling sites (P1, P2, and P3) and seasons (wet and dry) were assessed by a variance analysis (ANOVA). Data distribution normality of was first verified applying Shapiro-Wilk. Non normally distributed variables were log-transformed to fit a normal distribution. A statistical significance of $\alpha < 0.05$ was used for all statistical analyses. Pearson's correlation coefficient was employed to determine the strength of the associations between each pair of variables, where correlation coefficients higher

than 0.5 were interpreted as significant.

3. Results

3.1. Sediment geochemistry

Sedimentary compositions and OM sources at each sampling site were previously characterized by Matos et al. (2020), and the mean values \pm standard deviations are presented in Table 1. The estuarine mudflat (P1) presented very different sedimentary characteristics compared to the creek mudflats (P2 and P3). Located in the lowest topographic area, P1 exhibited a slightly higher sedimentation rate (1.8 cm yr^{-1}). Its grain size, however, is represented by a higher sand content ($\sim 52\%$) and significant contributions from marine OM (wet: 76.4% and dry: 79.6%). Both P2 and P3 are located in topographically higher tidal flats ($\sim 2 \text{ m amsl}$), where sediments are strongly oxidized during the dry season. The P2 site is located in a more confined area, presenting a lower sedimentation rate of 1.3 cm yr^{-1} , finer grain size of $\sim 68\%$ (silt + clay) and marine OM contributions of 54.5% in the wet season and 69% in the dry season. The P3 site, located closer to the mainland, presented a sedimentation rate of 1.5 cm yr^{-1} , finer particle size of $\sim 66\%$ and marine OM contributions of 60% in the wet season and 78% in the dry season.

Sediment-depth profiles of TOC, Fe_{S_2} , Fe_R and Mn_R in different seasons are presented in Fig. 2, and the mean values \pm standard deviation are displayed in Table 1. Sediment concentrations were different between sites, seasons, and depth. Overall, the TOC, Fe_{S_2} , Fe_R and Mn_R ranges were lower at site P1 compared to the sites P2 and P3. At all three sites, TOC concentrations decreased slightly with depth, ranging from 3.84 to 0.53%. Fe_{S_2} content showed large fluctuations between the sites and seasons varying from 0.06 to 1.52%, with the highest concentrations during the wet season. AVS concentrations were below the detection limit ($< 0.01 \text{ wt}\%$) in all sediment profiles. At P1, Fe_R concentrations in both seasons decreased slightly with depth, varying from 0.43 to 0.11%. At P2 and P3, Fe_R and Mn_R concentrations presented a clear seasonal trend, with the lowest Fe_R concentrations (0.34% at -16 cm to P2 and 0.34% at -8 cm to P3) determined during the wet season, and the highest concentrations (0.76% at -16 cm to P2 and 1.07% at -8 cm to P3) found in the dry. Mn_R concentrations ranged from 0.004 to 0.061%, and presented almost the same depth distribution patterns as Fe_R , with one peak of 0.044% at -20 cm to P2 and another of 0.061% at -8 cm to P3.

3.2. Physicochemical characteristics

Depth salinity, pH, and Eh profiles in the overlying and pore waters in different seasons are presented in Figs. 3–5. A clear seasonal signal was noted through the upper -15 cm , with the highest values detected in the dry season compared to the wet season. In the wet season, the overlying water salinity was of, on average, 4, and pore water salinity increased with depth (5–20 at P1, 4–13 at P2, and 4–15 at P3). In the dry season, the overlying water salinity was of, on average, 23, and pore

Table 1
Sedimentary characteristics of the P1, P2 and P3 sampling sites, during the wet and dry seasons.

Properties	P1		P2		P3		References
	Wet	Dry	Wet	Dry	Wet	Dry	
FeR (%)	0.25 \pm 0.6	0.29 \pm 0.8	0.59 \pm 0.11	0.54 \pm 0.14	0.63 \pm 0.18	0.48 \pm 0.07	This study
MnR (%)	0.016 \pm 0.003	0.007 \pm 0.003	0.029 \pm 0.006	0.016 \pm 0.005	0.030 \pm 0.011	0.020 \pm 0.003	
TOC (%)	0.9 \pm 0.3	1.3 \pm 0.2	3.4 \pm 0.3	2.6 \pm 0.2	2.7 \pm 0.2	2.5 \pm 0.2	Matos et al. (2020)
Sand (%)	51.7 \pm 10.4	52.6 \pm 5.6	36.8 \pm 7.4	26.5 \pm 7.7	32.4 \pm 10.3	35.6 \pm 8.9	
Silt (%)	46 \pm 9.3	46.3 \pm 5.3	58 \pm 6.6	71.5 \pm 6.9	60.2 \pm 9.3	62.2 \pm 8.6	
Clay (%)	2.3 \pm 1.3	1.0 \pm 0.4	5.2 \pm 1.0	2.0 \pm 1.0	7.4 \pm 1.5	2.2 \pm 0.5	
OM _{terr} (%)	23.6 \pm 6.0	20.4 \pm 6.2	45.5 \pm 3.4	31.0 \pm 9.5	40.1 \pm 3.9	21.8 \pm 8.7	
OM _{mar} (%)	76.4 \pm 6.0	79.6 \pm 6.2	54.5 \pm 3.4	69.0 \pm 9.5	59.9 \pm 3.9	78.2 \pm 8.7	
SAR ($cm \cdot yr^{-1}$)	1.8		1.3		1.5		

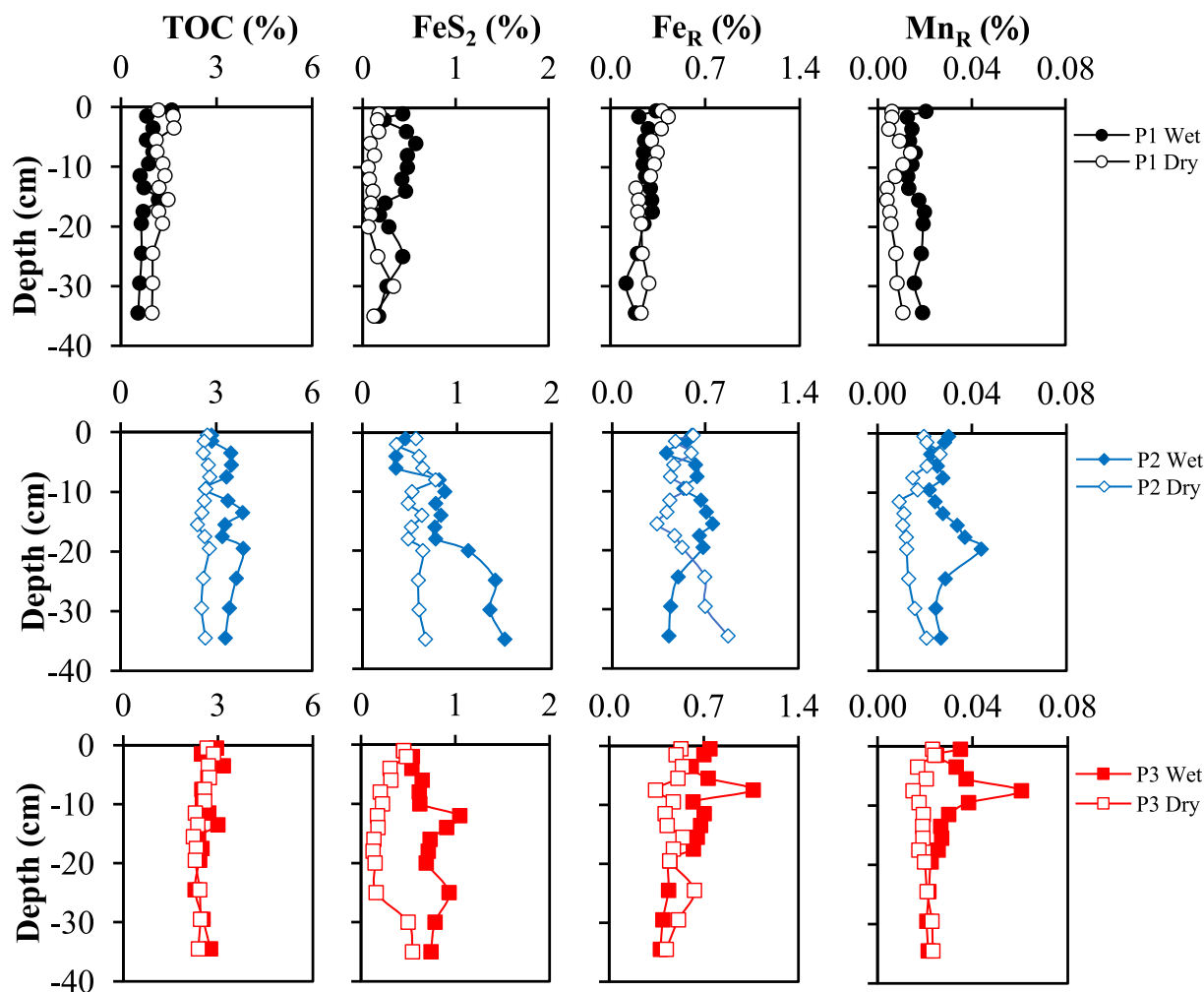


Fig. 2. Sediment TOC, FeS_2 , Fe_R and Mn_R profiles at the P1 (black), P2 (blue) and P3 (red) sampling sites during the wet (solid markers) and dry (open markers) seasons. (For interpretation of the references to color in this figure legend, the reader is referred to the Web version of this article.)

water salinity exhibited a distinct vertical pattern, decreasing with depth (24–19 at P1, 22–18 at P2 and 25–20 at P3). Furthermore, a significant difference between sampling sites was observed during the dry and wet seasons ($p < 0.05$). At P1, salinity remained constant below –18 cm in both seasons, while P2 and P3 exhibited stable salinity values below –35 cm in depth.

pH values were slightly acidic to neutral (6.7–7.4), and no seasonal variations were observed for the overlying water. Pore water pH values decreased with depth below the SWI during the wet season. In contrast, pH values slightly increased with depth during the dry season. The determined pH values were slightly more acidic during the wet season (5.9–6.5 at P1, 5.3–6.0 at P2 and 4.7–6.0 at P3) compared to the dry season (6.6–7.3 at P1, 6.7–7.2 at P2 and 6.6–7.0 at P3). Eh values in the overlying water were suboxic in both seasons at all sites, ranging from 40 to 190 mV. Eh values dropped very strongly from the SWI and tended to decrease with depth, ranging from –357 to –80 at P1, –220 to –125 at P2, and –180 to –95 at P3 in the wet season and from –146 to 0 at P1, –222 to –85 at P2 and –265 to –55 at P3 in the dry season. A significant seasonal difference was noted only for P1 ($p < 0.05$), which exhibited more reducing conditions during the wet season, and no significant seasonal differences were observed for the other sites ($p > 0.05$).

3.3. Pore water dissolved species profiles

Overlying and pore water profiles concerning Cl^- , SO_4^{2-} , redox-sensitive trace metals (Fe^{2+} and Mn^{2+}), total alkalinity (TA), sulfate

depletion ($\text{SO}_4^{2-}_{\text{Dep}}$), and nutrients (NH_4^+ and PO_4^{3-}) at three sampling sites during the wet and dry seasons are shown in Figs. 3–5. The Cl^- concentrations were positively correlated with salinity values at all sites and in both seasons ($0.81 < r < 0.91$, Supplementary Tables S1 and S2). At all sites, Cl^- concentrations increased from the overlying water to the pore water depth during the wet season (90–294 mM at P1, 59–143 mM at P2 and 54–314 mM at P3) and decreased with depth during the dry season (332–260 mM at P1, 317–260 mM at P2 and 376–310 mM at P3). The SO_4^{2-} concentrations exhibited a similar trend regarding salinity only during the dry season, with decreasing concentrations from the overlying water to the pore water with depth (16.0–7.5 mM at P1, 13.1–6.8 mM at P2 and 13.6–6.6 mM at P3). During the wet season, however, the downcore pore water SO_4^{2-} concentrations displayed different characteristics at each site (Figs. 3–5).

During the wet season, sites P1, P2, and P3 featured the highest pore water Fe^{2+} concentrations closer to the SWI, reaching 285.1, 198.8, and 170.1 μM , respectively. During the dry season, pore water Fe^{2+} concentrations were very low in the upper centimeters, followed by a 275 μM peak in –10 cm at site P1, 140.2 μM in –4 cm at site P2, and 219.3 μM in –4 cm at site P3. During the wet season, pore water Mn^{2+} concentrations were also higher closer to the SWI, except for P3, reaching 72.2 at site P1 and 53 μM at P2, respectively. During the dry season, Mn^{2+} peaks were located above the Fe^{2+} peaks, reaching 86.7 μM in –8 cm at site P1, 104.7 μM in –4 cm at site P2 and 175.7 μM in –4 cm at site P3. Fe^{2+} and Mn^{2+} concentrations drastically decreased below the peaks with increasing depths at the three sampling sites.

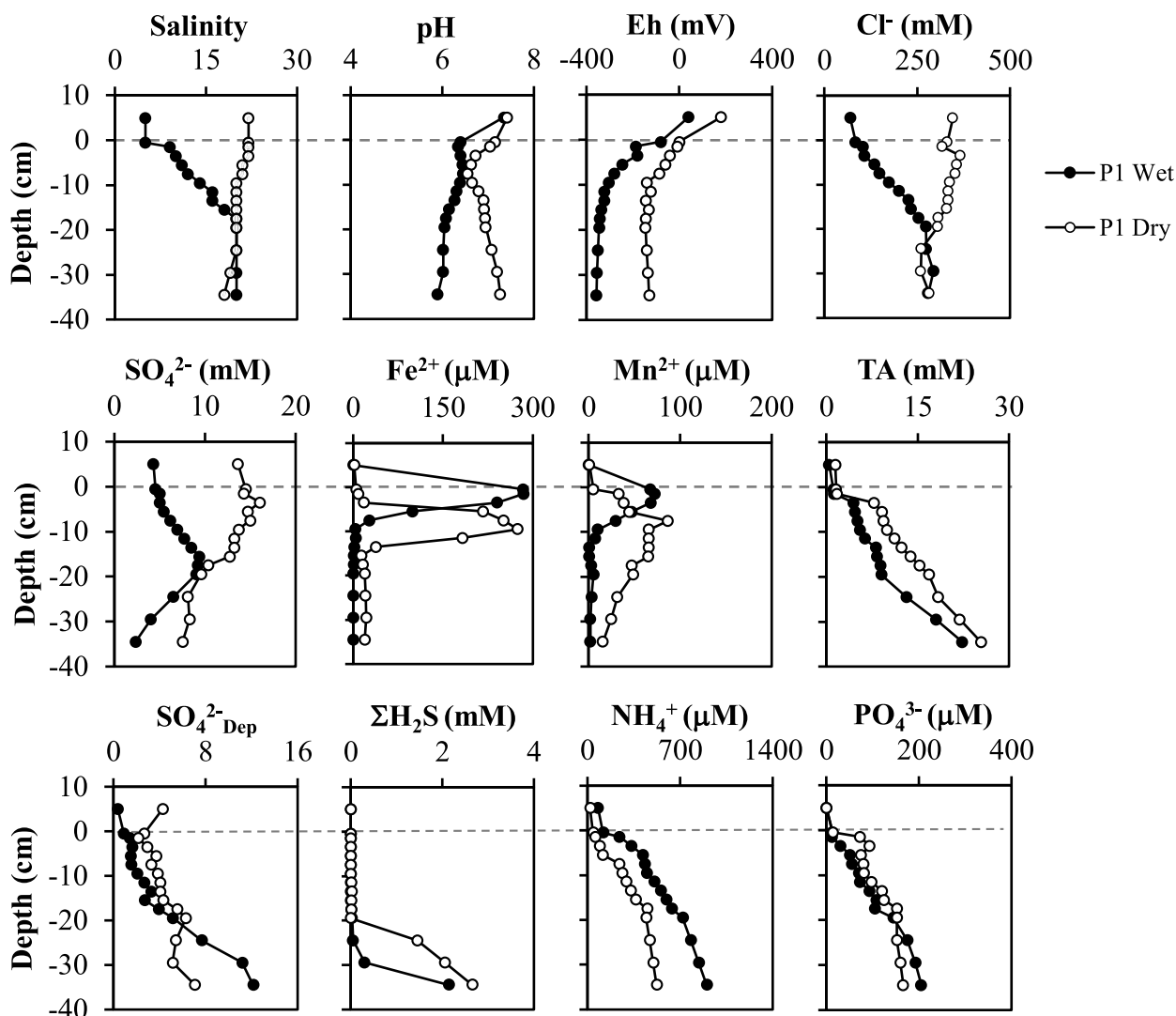


Fig. 3. Overlying and pore water profiles concerning physicochemical parameters (salinity, pH and Eh), Cl^- , SO_4^{2-} , redox-sensitive trace metals (Fe^{2+} and Mn^{2+}), total alkalinity (TA), sulfate depletion ($\text{SO}_4^{2-}\text{-Dep}$) and nutrients (NH_4^+ and PO_4^{3-}) at sampling site P1 during the wet (filled circles) and dry (open circles) seasons. Dashed horizontal lines represent the SWI.

TA concentrations varied from 0.4 to 2.0 mM in the overlying water, and increased sharply with depth below the SWI, ranging from 1.1 to 25.4 mM. Pore water TA concentrations did not differ significantly between seasons ($p > 0.05$). The $\text{SO}_4^{2-}\text{-Dep}$ values increased with sediment depth at all sites, ranging from 0.6 to 12.1. $\text{SO}_4^{2-}\text{-Dep}$ did not differ considerably between sites ($p > 0.05$), but were significantly different between seasons at sites P2 and P3 ($p < 0.05$), exhibiting slightly higher values in the dry season. Pore water $\Sigma\text{H}_2\text{S}$ concentrations at P2 and P3 were negligible ($< 1 \mu\text{M}$), while a high peak of 2 mM was recorded at the -35 cm depth at site P1.

NH_4^+ concentrations varied from 3.1 to 79.2 mM in the overlying water. The pore water NH_4^+ range was highest at sites P1 (119.2–900.8 μM), and P2 (286.2–1083.8 μM) compared to site P3 (72.5–349.2 μM). Seasonal patterns were significant ($P < 0.05$) only at P1 and P2, where pore water concentrations were higher in the wet season. Pore water NH_4^+ concentrations increased with sediment depth at all sites. PO_4^{3-} concentrations ranged from 0.2 to 1.0 mM in the overlying water. Pore water PO_4^{3-} concentrations were not significantly different between seasons ($p > 0.05$), while differing significantly between sites ($p < 0.05$), with the highest concentrations at P2 (1.2–342.9 μM) compared to P1 (12.5–205.0 μM) and P3 (1.2–227.5 μM).

3.4. Metal and nutrient fluxes at the sediment-water interface (SWI)

The diffusive metal and nutrient fluxes estimates at the SWI at the three sites during the wet and dry seasons are exhibited in Table 2. The Fe^{2+} , Mn^{2+} , NH_4^+ , and PO_4^{3-} fluxes in both seasons at all sites were positive, indicating sediment pore water exports to the overlying water. Overall, Fe^{2+} , Mn^{2+} , NH_4^+ , and PO_4^{3-} exhibited the highest fluxes in the wet season, except for Mn^{2+} at site P3. Fe^{2+} , Mn^{2+} , NH_4^+ , and PO_4^{3-} fluxes ranged from 6 to 723 $\mu\text{mol m}^{-2} \text{d}^{-1}$, from 16 to 189 $\mu\text{mol m}^{-2} \text{d}^{-1}$, from 90 to 1,433 $\mu\text{mol m}^{-2} \text{d}^{-1}$, and from 2 to 35 $\mu\text{mol m}^{-2} \text{d}^{-1}$, respectively (Table 2).

Positive numbers indicate fluxes from the sediment (effluxes) and negative numbers indicate fluxes to the sediment (influxes).

4. Discussion

4.1. Seasonal physicochemical properties and Cl^- variabilities

Salinity oscillations detected herein were associated to seasonal rainfall rate variations. Due to increasing rainfall rates and runoff from the Marapanim River, surface salinity values were five times lower in the wet season relative to the dry season, indicating greater saline water

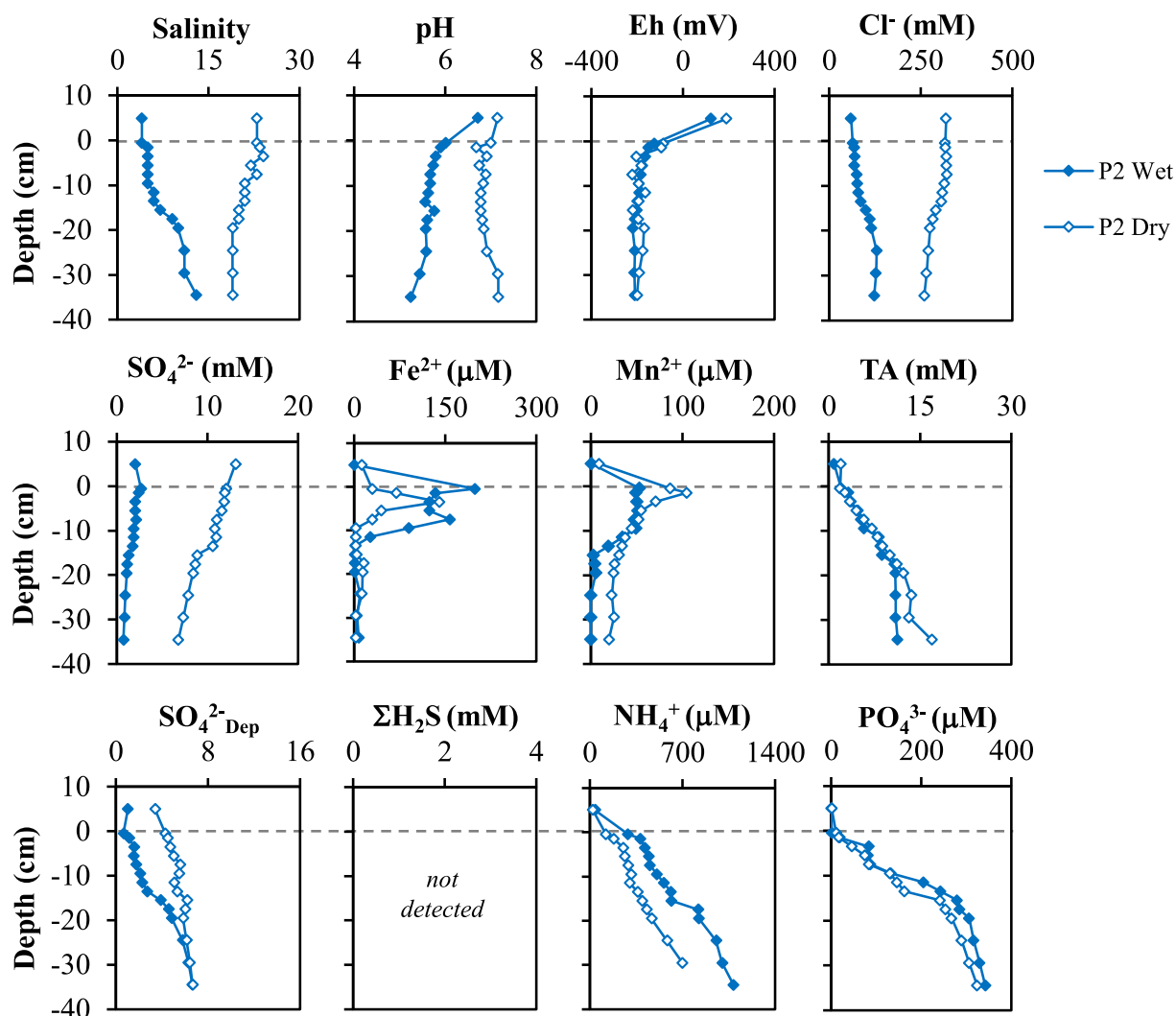


Fig. 4. Overlying and pore water profiles concerning physicochemical parameters (salinity, pH and Eh), Cl^- , SO_4^{2-} , redox-sensitive trace metals (Fe^{2+} and Mn^{2+}), total alkalinity (TA), sulfate depletion ($\text{SO}_4^{2-}\text{Dep}$) and nutrients (NH_4^+ and PO_4^{3-}) at sampling site P2 during the wet (filled circles) and dry (open circles) seasons. Dashed horizontal lines represent the SWI.

dilution by freshwater, as observed at the Sinnamary mangrove by Marchand et al. (2004) and at the Marapanim mangrove by Berrêdo et al. (2016). The seasonal effects controlled the conservative Cl^- and salinity values, especially in the upper sediment intervals (<15 cm). Spatial variations were observed only during the wet season, with lower salinity and Cl^- values detected at the creek mudflats (P2 and P3) compared to the estuarine mudflat (P1). Spatial salinity and Cl^- variabilities can be explained by spatial grain size variability. The fine-grained sediments identified at P2 and P3 promote high freshwater retention capacity, while P1, characterized by sandy sediments (>50%), favored saline water recharge during rising tides. At P1, pore water salinity remained constant below -18 cm in both seasons, while pore water salinity remained constant below the -35 cm depth at P2 and P3.

The increased rainfall trend observed during the wet season led to a decrease in pH values, which may be explained by a more intense OM decomposition, as well as the reoxidation of reduced products that result in lower pH (Gueiros et al., 2003; Otero et al., 2006), such as Fe sulfide (pyrite, FeS) and pore water sulfide (HS) oxidation during the wet season. Acidity was higher at P2 and P3, reaching values lower than 5 (Figs. 4–5). These sites are located in topographically higher areas, leading to strong sediment oxidation. Sediments more acidic during the wet season have been reported in other tropical intertidal environments (Alongi et al., 1999, 2004). During the dry season, saline water

recharges influence pore water quality, buffering the pH close to neutrality (6.6–7.3), with no significant difference noted between sites. Redox potential values indicate suboxic to anoxic conditions at all sampling sites. Eh values were very sensitive to seasonal changes only at site P1, significantly lower in the wet season than dry season (Fig. 3).

4.2. Biogeochemical processes and seasonal variations

Irrespective of the pathways, all mangrove OM not exported by tidal action enters the sediment and is degraded or chemically modified by microorganisms (Kristensen et al., 2008). Microbes in the sediment surface use electron acceptors (for example, O_2 , MnO_2 , Fe-oxides, SO_4^{2-}) in order of declining energy yields from OM respiration (Froelich et al., 1979). High OM accumulation in mangrove sediments enhances intense microbial activity, sedimentary mineralization rates are high, often leading to oxygen depletion within the upper few sediment millimeters (Glud, 2008; Kristensen et al., 1994; Meiggs and Taillefert, 2011) and favoring the prevalence of anaerobic OM mineralization pathways, such as iron reduction and sulfate reduction (Alongi, 1995; Kristensen et al., 2011).

The gradual decrease observed for TOC concentrations and redox potential with depth in all sampled cores likely reflect microorganisms OM degradation. The pore water profiles allowed for the assessment of

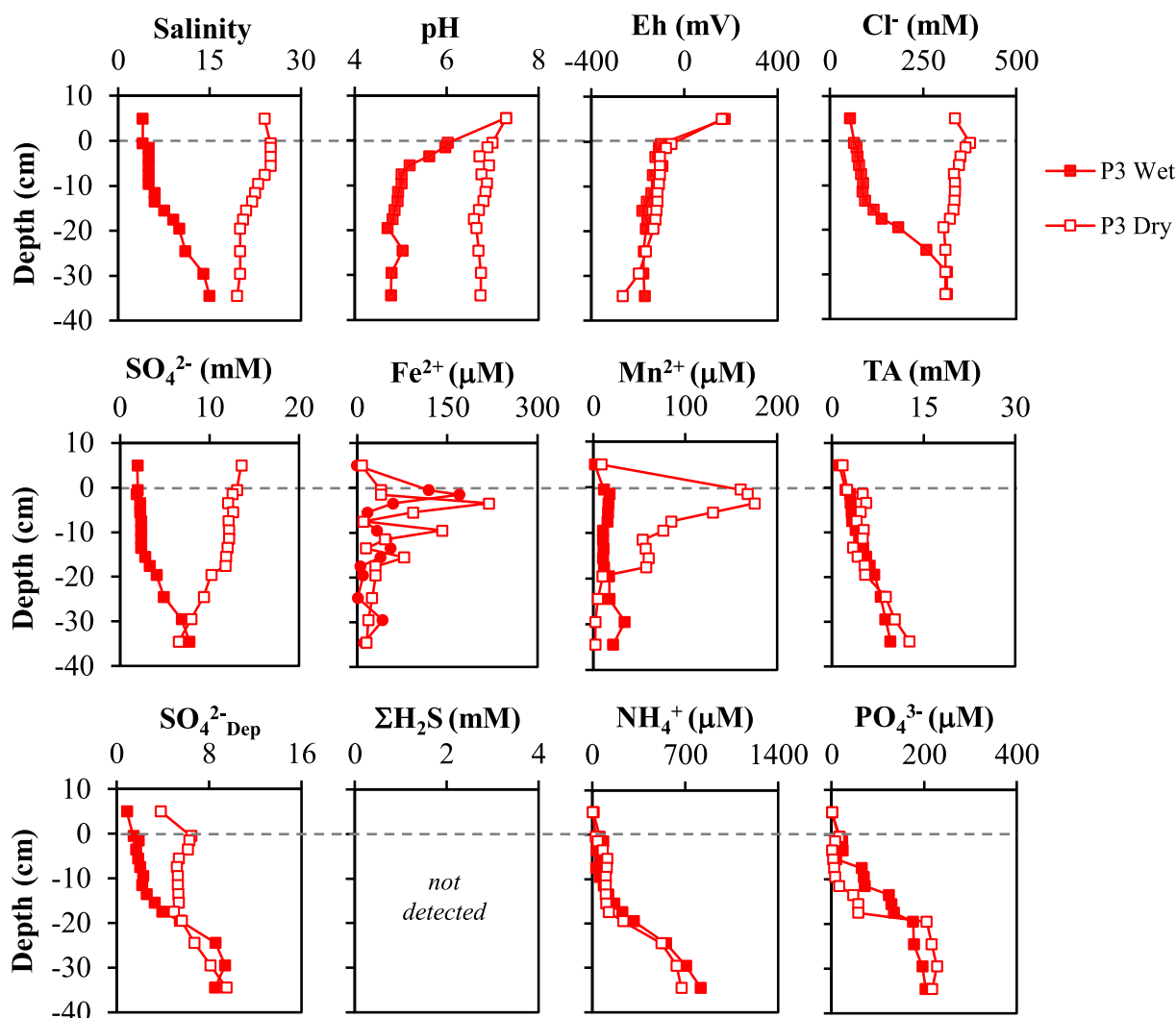


Fig. 5. Overlying and pore water profiles concerning physicochemical parameters (salinity, pH and Eh), Cl^- , SO_4^{2-} , redox-sensitive trace metals (Fe^{2+} and Mn^{2+}), total alkalinity (TA), sulfate depletion ($\text{SO}_4^{2-}\text{-Dep}$) and nutrients (NH_4^+ and PO_4^{3-}) at sampling site P3 during the wet (filled circles) and dry (open circles) seasons. Dashed horizontal lines represent the SWI.

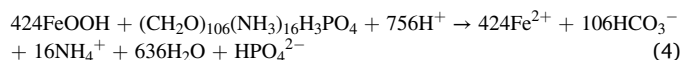
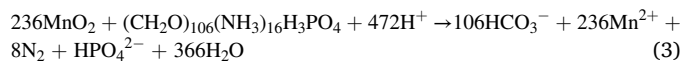
Table 2

Fe^{2+} , Mn^{2+} , NH_4^+ , and PO_4^{3-} fluxes ($\mu\text{mol m}^{-2} \text{d}^{-1}$) across the SWI at sampling sites P1, P2 and P3, during the wet and dry seasons.

	P1		P2		P3	
	Wet	Dry	Wet	Dry	Wet	Dry
Fe^{2+}	723	6	595	24	238	75
Mn^{2+}	92	32	73	64	16	189
NH_4^+	415	90	1,433	155	201	121
PO_4^{3-}	24	18	35	14	19	2

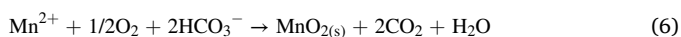
the redox sequence associated to OM mangrove mudflat sediment degradation. Based on downcore Fe^{2+} and Mn^{2+} variations, the sediment cores were subdivided into two distinct zones, as follows: Zone 1 (from 0 to -15 cm) presents peaks with high dissolved Fe^{2+} and Mn^{2+} concentrations, revealing a suboxic zone in these sediments. This mobilization is due to Fe and Mn oxyhydroxides use as terminal electron acceptors in bacterial OM oxidation (Eqs. (3) and (4)) (Froelich et al., 1979), resulting in decreased Mn_R and Fe_R concentrations (referred to in the equations as MnO_2 and $\text{FeOOH}/\text{Fe}(\text{OH})_3$) in the solid-phase in this zone (Fig. 2). High Mn^{2+} and Fe^{2+} concentrations depth sequences were recorded during the dry season, as Mn^{2+} appeared vertically in solution before Fe^{2+} . However, during the wet season, Mn^{2+} and Fe^{2+} appeared

simultaneous and closer to the SWI, probably due to strong resuspension and the effect of tidal pumping caused by intense rainfall rates. Marchand et al. (2006) also observed Fe^{2+} and Mn^{2+} variations with depth associated to seasonal fluctuations.

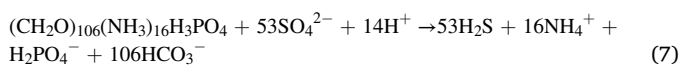


Pore water Fe^{2+} reached higher concentrations at P1 (285.1 μM) compared to P2 (198.8 μM) and P3 (219.3 μM). Although freshwater discharge penetration during the wet season significantly decreased pH values, which would enhance oxyhydroxide dissolution (Holloway et al., 2016; Otero et al., 2009), the highest Fe^{2+} concentrations did not indicate significant difference between seasons, probably due to the high Fe supply from the continent (Barreiras Formation, Vilhena et al., 2010). However, Fe^{2+} peaks were typically deeper during the dry season. Low Fe^{2+} concentrations were observed at the top pore water (0 to -2 cm) during the dry season, increasing in the surface solid phase, probably due to Fe^{2+} oxidation and precipitation in the form of oxyhydroxides, likely associated to high oxygen sediment exposure during the low tide due to lower river discharges.

During tidal oscillations, multiple reduction-oxidation reactions may occur, and Fe^{2+} and Mn^{2+} may be removed from the pore water by oxidation to form oxyhydroxides (Liu et al., 2019), which explains the Fe_R and Mn_R peaks around -20 cm at P2 and -8 cm at P3 during the wet season (Fig. 2). A percentage of the dissolved Fe and Mn encounters oxygen from the sediment surface and precipitates back to Mn and Fe oxyhydroxides (Eqs. (5) and (6)). These peaks also seem to mark the transition zone between suboxic and anoxic phases. Only pore water Mn^{2+} at P3 showed much lower concentrations during the wet season, consistent with higher reactive Mn_R concentrations in the solid-phase (Fig. 2). At this site, Mn_R precipitation was probably enhanced by bioturbation activities. Sediment mixing (i.e. physical or/and biological mixing) was noted in the surface sediment layers at P3, determined through the excess ^{210}Pb profiles reported by Matos et al. (2020), masking the production of pore water Mn^{2+} at the SWI. This mixing can also explain the top pore water Fe^{2+} concentration variations observed at P3. Gueiros et al. (2003) also observed higher Mn^{2+} profile intensities during the dry season compared to wet season in mudflat sediments. On the other hand, Thanh-Nho et al. (2020) and Lacerda et al. (1999) observed the highest dissolved Mn concentrations during the wet season.



In zone 2 (below -15 cm), the concurrent decreases in Fe^{2+} and Mn^{2+} were accompanied by a steady increase in TA, SO_4^{2-} Dep, PO_4^{3-} and NH_4^+ toward the base of the core, suggesting an anoxic zone, with rapid OM mineralization in deeper sediment layers (Figs. 3–5). Regression analyses between SO_4^{2-} Dep as an estimate for the metabolic amount of sulfate reduction (SR) and TA as a terminal metabolic product were performed. According to Eq. (7), where OM is sourced from phytoplankton (Redfield et al., 1963), OM degradation is mainly related to SR. Thus, a TA: SO_4^{2-} Dep ratio of 2 would be expected. SO_4^{2-} Dep in pore waters was positively correlated to total alkalinity at all sites (see Supplementary Tables S1 and S2). The TA: SO_4^{2-} Dep ratio revealed by the regression analysis slope ranged between 1.0 and 2.6. According to the Redfield ratio, this range indicates sulfate reducing conditions.



Considering the pore water is devoid of free sulfide at sites P2 and P3, and appear at site P1 only in deeper layers, a tight coupling between sulfide production via SR and sulfide consumption by pyrite formation may be proposed (Raiswell and Canfield, 1998). The $\Sigma\text{H}_2\text{S}$ can react with Fe^{2+} and Fe_R to form iron sulfides, e.g., FeS (Eq. (8)) and FeS_2 (Eq. (9)). However, the low $\Sigma\text{H}_2\text{S}$ and AVS (mainly FeS) concentrations can also be due to intense oxidation and pore water exchange during the exposure of the tidal mudflats at the low tides as result of tidal pumping. As reported by Pan et al. (2019b) the formation and reoxidation of sulfide along the surface layers within the intertidal zones are likely regulated by tide-induced redox changes.

In the wet season, when the reducing conditions become pronounced, at sites P2 and P3 pyrite concentrations increase substantially in the solid phase below Fe^{2+} and Fe_R peaks (Fig. 2). Thus, the consumption of Fe_R and Fe^{2+} in deeper sediments occurs due to iron sulfide precipitation. Lower pyrite concentrations in the dry season, especially at sites P2 and P3 are probably due to these sites being located in topographically higher areas and their sediments are strongly oxidized during the dry season, promoting the pyrite oxidation (Eq. (10)), thus Fe_R concentrations increase with depth reaching higher concentrations in the dry season than the wet season in deeper sediment layers. The oxidation of Fe sulfides to Fe oxyhydroxides which occurred in the dry season is similar to the seasonal changes observed in other studies (Luther et al., 1992; Rozan et al., 2002). Pyrite oxidation was previously

observed in Marapanim mangrove sediments by Vilhena et al. (2010), they observed oxidation of pyrite grains surface and the presence of jarosite mineral as a product of pyrite oxidation. The Mn consumption in deeper layers is likely associated to pyrite coprecipitation, as reported in other studies (Huerta-Diaz, 1992; Otero and Macias, 2003; Santos-Echeandia et al., 2009).



Seasonal effects, mainly controlled by freshwater discharges, affected the downcore profiles of pore water SO_4^{2-} Dep in the investigated sediments. Sulfate depletion was not appreciable in the top sediment layers (above -15 cm) at all sites during the wet season, due to the dilution-mixing process, that results in a more efficient sulfate removal than bacterial SR in these layers. On the other hand, sulfate depletion increased abruptly below the dilution-mixing layers. Similar seasonal trends were also reported by Wu et al. (2015) at the Pearl River estuary. SR products (TA, NH_4^+ and PO_4^{3-}) indicated no simple mixing trend in the dilution-mixing layer (Figs. 3–5), suggesting that pore waters TA, NH_4^+ and PO_4^{3-} are substantially altered by diagenetic reactions, such as Fe and Mn reduction. However, only pore water NH_4^+ exhibited any seasonal variability, with the highest concentrations detected in the wet season. A similar phenomenon was reported by Meiggs and Taillefert (2011), who investigated seasonal effects on estuarine sediments biogeochemical processes, indicating that dilution-mixing does not cause seasonal SR product alterations.

Suboxic to anoxic sediment conditions limit aerobic OM degradation. Iron reduction and SR are energetically less favorable degradation processes, thus enhancing OM burial. As previously observed by Matos et al. (2020), the sampling sites exhibit higher potential regarding TOC, TN and TP sediment accumulation, especially the creek mudflats (P2 and P3). The mudflat sediment in the Marapanim River margin (site P1) presented lower TOC, higher sand contents and high marine OM contributions compared to P2 and P3 (Table 1). P1, however, reached higher terminal metabolic end-products of OM mineralization concentrations, such as Fe^{2+} , SO_4^{2-} Dep, H_2S and TA, suggesting that the OM of this estuarine mudflat is more susceptible to degradation compared to the mangrove creek mudflats. Typically, organic-rich sediments present high OM degradation rates. However, due to the enhanced OM and oxygen input by advective processes at the sediment surface, sandy sediments containing low organic carbon contents often exhibit OM degradation rates comparable to organic-rich muds (Beck et al., 2008; Rusch et al., 2006). OM degradation rates further depend on sedimentary OM sources. For example, previous studies have demonstrated that marine-derived OM (fresher or more labile) is more susceptible to degradation by microorganisms than terrestrial OM (more refractory) (Hedges et al., 1997; Matos et al., 2020; Ranjan et al., 2011). Therefore, coarse-textured sediment and higher available labile OM likely contributed to more susceptible OM degradation at P1, resulting in low TOC concentrations.

4.3. Seasonal diffusive flux variability at the SWI

High amounts of Fe^{2+} and Mn^{2+} are produced by microbial Fe and Mn reduction processes, respectively, which then diffused from the sediment pore waters into the overlying water, indicating that the studied mudflats comprise a source of Fe^{2+} and Mn^{2+} . The changes in diagenetic processes induced by increasing rainfall rates, therefore, lead to variable diffusive fluxes. Concerning the wet season, the highest Fe^{2+} concentration was noted just below SWI, generating higher fluxes during this period (Table 2). On the other hand, Fe^{2+} concentrations in the dry season were lower in the top sediment layers, probably due to high oxygen sediment exposure during the low tide, enhancing oxidized solid

phase severely limiting its diffusion to the overlying water. Mn^{2+} fluxes followed the same trend as Fe^{2+} fluxes, except at P3, which presented lower fluxes in the wet season due to sediment mixing, resulting lower Mn^{2+} concentrations in the surface sediment. Marchand et al. (2006) also reported higher dissolved Fe and Mn fluxes in the wet season compared to dry season, as a result of vertical redox status oscillations.

Sediment pore waters constituted a source of PO_4^{3-} and NH_4^+ to the water column at all sites, with higher fluxes in the wet compared to the dry season (Table 2). As reported by Taillardat et al. (2019), intense rainfall events reduce pore water salinity and enhance OM degradation, which is likely to increase phosphate and nitrogen mineralization. The high NH_4^+ pore water concentrations and the strong correlation between NH_4^+ and SO_4^{2-} Dep pore water detected in both sampling seasons ($r = 0.61$ – 0.70 , Supplementary Tables S1 and S2) reveal high OM mineralization (ammonification), more intense during the wet season, with higher downcore pore water concentrations. Mangrove sediments generally comprise NH_4^+ sinks (Alongi, 2020b and references within), mostly due to N- NH_4^+ uptake by vegetation, although an efflux for NH_4^+ is often noted (Gleeson et al., 2013; Matos et al., 2016; Sadat-Noori and Glamore, 2019; Tait et al., 2017), as observed herein for the investigated mangrove mudflats, as no permanent macrophytic vegetation in the mudflat is available to consume dissolved nutrients (Taillardat et al., 2019).

Pore water PO_4^{3-} concentrations were also significantly and positively correlated with SO_4^{2-} Dep pore water in the wet season ($r = 0.64$, Supplementary Table S1). This positive correlation receded in the dry season ($r = 0.48$, Supplementary Table S2), due to enhanced SO_4^{2-} Dep in the upper layers, that did not affect downcore pore water PO_4^{3-} . Other studies have indicated that the release or adsorption of P in coastal sediments is associated with the iron redox cycle (Ding et al., 2016; Sherman et al., 1998). Fe oxy-hydroxides potentially adsorb P under more oxidizing conditions. In contrast, more reducing conditions favor its mobility from sediments to pore waters (Bava and Seralathan, 1999). However, low PO_4^{3-} remobilization in the upper layers where Fe reduction occurs implies that PO_4^{3-} release was not associated to Fe-bound P at our investigated study sites. A low negative correlation between PO_4^{3-} and Fe^{2+} , and significant positive correlations between PO_4^{3-} and NH_4^+ and TA (Supplementary Tables S1 and S2) reinforces the assumption that PO_4^{3-} release to pore water was mainly derived from OM mineralization by SR.

Overall, the short but remarkable climate fluctuations influenced pore water concentrations and physicochemical properties and, consequently, the intensity of metal and nutrient exchange rates at the SWI in our study sites. It is, therefore, essential to take consider local weather conditions when estimating and managing nutrient and metal budgets. Climatic variability (e.g., changes in rainfall and the frequency and intensity of storms) can exacerbate factors affecting mangrove responses to sea level, altering freshwater inflow to mangroves, sediment and nutrient inputs and salinity regime (Alongi, 2018; Mcleod and Salm, 2006). Studies in Bragança Peninsula, 110 km distant from the study area, indicated that mangroves have invaded higher tidal flats since 1984 due to a relative sea level rise (Cohen et al., 2009, 2018, 2021; Cohen and Lara, 2003).

Metals and nutrients fluxes at the SWI have been estimated in other mangrove systems worldwide (Supplementary Table S3), but their direction and intensity vary among sites. For example, diffusive Fe^{2+} fluxes in Marapanim mangrove mudflats are low compared to temperate mangrove creeks (Holloway et al., 2018; Sadat-Noori and Glamore, 2019), while diffusive Mn^{2+} fluxes present the same order of magnitude as those reported for other mangrove creeks (Holloway et al., 2016; Pan et al., 2019a). NH_4^+ and PO_4^{3-} fluxes are comparable to those determined in subtropical mangrove forest (Kaiser et al., 2015), temperate mangrove creeks (Tait et al., 2017) and tropical mangrove-fringed estuaries (Pratihary et al., 2021), but are lower than other subtropical mangrove creeks (Gleeson et al., 2013; Pan et al., 2019a, 2019b) and temperate mangrove wetlands (Sadat-Noori and Glamore, 2019). These

variations may be due to many factors, including differences in terrestrial or oceanic nutrient inputs, redox condition shifts, anthropogenic activities and local environmental factors, such as weather conditions, hydrology, tidal ranges, latitudes, mangrove community structures and topographic elevations (Adame et al., 2010; Adame and Lovelock, 2011; Kristensen et al., 2017). In addition, this comparison must be cautiously considered, due to different analysis methods and high inter-site variability.

4.4. Pore water solute flux versus depositional fluxes

The diffusive fluxes in $mmol\ m^{-2}\ d^{-1}$ were converted to $g\ m^{-2}\ yr^{-1}$ for comparisons to depositional fluxes. Total nitrogen and total phosphorous depositional fluxes were obtained from Matos et al. (2020). Fe and Mn depositional fluxes were estimated from reactive Fe and Mn concentrations, sediment accumulation and dry bulk density reported previously by Matos et al. (2020). The average between the three study sites, propagate to the average between the wet and dry season dataset, of the calculated diffusive fluxes from the pore water to the overlying water column for N (as NH_4^+), P (as PO_4^{3-}), Fe (as Fe^{2+}) and Mn (as Mn^{2+}) were 2.6, 0.5, 5.7, and $1.6\ g\ m^{-2}\ yr^{-1}$, respectively. Regarding N, P, Fe and Mn depositional fluxes were 15.3, 3.2, 42.3 and $1.8\ g\ m^{-2}\ yr^{-1}$, respectively (Table 3). The release of dissolved NH_4^+ , PO_4^{3-} , Fe^{2+} and Mn^{2+} from the pore water to the overlying water corresponds to averages of ~17, 16, 15 and 90% (% recycling) of the total amount of N, P, Fe and Mn deposited in the sediment (% burial), respectively (Table 3).

Marapanim mangrove sediments contain high Fe concentrations, with a mean of 6.5% (Vilhena et al., 2010). The reactive Fe concentrations found in these mudflat sediments correspond to <10% to those detected in the mangrove forest, highlighting Fe burial efficiency (85%) in Marapanim mudflats. In contrast, Berrêdo et al. (2008a) observed lower total Mn concentrations (0.03%) than those detected in the investigated mudflat, of 0.06%. This high recycling potential of ~90% corroborates with Holloway et al. (2016), who state that undisturbed mangrove creeks may be a major source of Mn^{2+} to coastal oceans. N and P burial efficiency (~84%) is driven by suboxic conditions, where Fe and Mn reductions appear to limit PO_4^{3-} and NH_4^+ pore water mobilization and their fluxes to overlying surface waters.

Intertidal mudflat sediments are submitted to intense oscillations associated to tidal heights, which may enhance dissolved nutrient and metal flows through by lateral tidal drainage, advection or groundwater transport (Holloway et al., 2016; Sanders et al., 2015; Tait et al., 2017). Thus, the low PO_4^{3-} and NH_4^+ pore water mobilization in the upper layers can also be due to tidal-induced pore water seepage from the upper layers into the creek water columns during low and ebbing tides. Pore water exchange can be reduced by geochemical factors such as absorption and precipitation (Ogrinc and Faganeli, 2006; Rozan et al., 2002). In our study, low dissolved metal concentrations and their low fluxes across the SWI during the dry season, affected by seasonal rainfall patterns, indicate considerable oxidation and metals trapping into solid-phases. Bioturbation activities can increase sediment oxygen and a fraction of the produced Fe^{2+} , Mn^{2+} and NH_4^+ may be oxidized in the upper layers where suboxic conditions are common. In contrast, crab burrows have been demonstrated to increase the hydraulic conductivity of mangrove sediments and create a larger effective surface area enhancing diffusive fluxes (Bouillon et al., 2007). Therefore, diffusive fluxes based only on molecular diffusion and gradient concentrations at the SWI represent only a minimal estimate of how these mudflat pore waters can act as a water column source.

5. Conclusions

The present study demonstrates that pore water concentrations, physicochemical properties, and the intensity of metal and nutrient exchange rates at the SWI in intertidal mudflat sediments fringed by pristine mangroves in northern Brazil are influenced by Amazonian

Table 3Upward diffusive NH_4^+ , PO_4^{3-} , Fe^{2+} and Mn^{2+} fluxes and depositional total N and P and reactive Fe and Mn fluxes at P1, P2, and P3 sampling sites.

Site	Diffusive flux				Depositional flux				Recycling				Burial			
	(g m ⁻² yr ⁻¹)				(g m ⁻² yr ⁻¹)				N		Mn		N		Mn	
	N	P	Fe	Mn	N	P	Fe	Mn	%	P	%	P	%	Fe	Mn	
P1	1.4	0.7	7.5	1.3	11.0	2.7	37.2	1.8	12.8	27.2	18.6	70.2	87.2	72.8	81.4	29.8
P2	5.2	0.4	6.3	1.4	16.4	3.1	42.7	1.6	31.9	11.7	18.8	86.1	68.1	88.3	81.2	13.9
P3	1.1	0.4	3.2	2.1	18.4	3.9	47.0	2.1	5.8	9.4	6.7	112.3	94.2	90.6	93.3	-12.3
Average	2.6	0.5	5.7	1.6	15.3	3.2	42.3	1.8	16.8	16.1	14.7	89.5	83.2	83.9	85.3	10.5

seasonal rainfall patterns. A seasonal shift from the dry to the wet season was observed, with increasing acidic and reducing conditions, pore water salinity declines, and increased elemental concentrations within the pore water and sediments. The redox zonation of sediments oscillated vertically in response to rainfall patterns, affecting pore water species and their fluxes across the sediment-water interface. Under suboxic conditions, the mudflat pore waters constitute a source of Fe^{2+} , Mn^{2+} , NH_4^+ and PO_4^{3-} to the water column, and the magnitude of these effluxes increased in the wet season. However, when compared with burial fluxes, the release of dissolved NH_4^+ , PO_4^{3-} , Fe^{2+} and Mn^{2+} from the pore water to the overlying water corresponded to ~17, 16, 7 and 90% of the amount of TN, TP, Fe_R and Mn_R deposited in the sediment, respectively. This demonstrates that Marapanim mudflats are effective in retaining nutrients and Fe in their sedimentary solid phases compared to coastal water exports, while also potentially comprising significant Mn contributor to coastal waters. These findings evidence the role of mangrove-fringed tidal creeks as sites exhibiting intense biogeochemical processes, rather than simple dissolved material routes between mangroves and coastal oceans, which are strongly influenced by rainfall events.

Funding

This work was supported in part by CAPES (Finance code 001) and by Brazilian Research Council (CNPq). C.J. Sanders is supported by the Australian Research Council (DE160100443), E. Metzger by CNRS-EC2CO project Vubleu, and W. Machado by CAPES-Print-Feedbacks Project (Proc. No. 88887.310301/2018-00).

Authors's contributions

All authors made substantial contributions to the conception, design, and acquisition of data. CRLM wrote first draft and all authors commented on the previous versions of the manuscript, critically revising and adding important intellectual content. All authors approved the final version.

Declaration of competing interest

The authors declare that they have no known competing financial interests or personal relationships that could have appeared to influence the work reported in this paper.

Acknowledgments

The authors thank the research grants from the Brazilian Ministry of Education (CAPES) and the Brazilian Research Council (CNPq) to the first author C.R.L. Matos. C.J. Sanders is supported by the Australian Research Council (DE160100443) and E. Metzger by CNRS-EC2CO project Vubleu. W. Machado thanks the CAPES-Print-Feedbacks Project (Proc. No. 88887.310301/2018-00). Rut Diaz from Universidade Federal Fluminense (UFF) is thanked for her assistance with the pyrite analysis. The authors also acknowledge the Evandro Chagas Institute (IEC) and Museu Goeldi (MPEG) for the use of their facilities.

Appendix A. Supplementary data

Supplementary data to this article can be found online at <https://doi.org/10.1016/j.apgeochem.2022.105217>.

References

- Adame, M.F., Lovelock, C.E., 2011. Carbon and nutrient exchange of mangrove forests with the coastal ocean. *Hydrobiologia* 663, 23–50. <https://doi.org/10.1007/s10750-010-0554-7>.
- Adame, M.F., Virdis, B., Lovelock, C.E., 2010. Effect of geomorphological setting and rainfall on nutrient exchange in mangroves during tidal inundation. *Mar. Freshw. Res.* 61, 1197–1206. <https://doi.org/10.1071/MF10013>.
- Alongi, D.M., 2020a. Global significance of mangrove blue carbon in climate change mitigation (version 1). *Science* 2, 1–15. <https://doi.org/10.3390/sci2030057>.
- Alongi, D.M., 2020b. Nitrogen Cycling and Mass Balance in the World ' S Mangrove Forests 167–189.
- Alongi, D.M., 2018. Impact of global change on nutrient dynamics in Mangrove Forests. *Forests* 9, 1–13. <https://doi.org/10.3390/f9100596>.
- Alongi, D.M., 1995. Decomposition and recycling of organic matter in muds of the Gulf of Papua, northern Coral Sea. *Continental Shelf Res.* 15, 1319–1337. [https://doi.org/10.1016/0278-4343\(94\)00087-4](https://doi.org/10.1016/0278-4343(94)00087-4).
- Alongi, D.M., Tirendi, F., Dixon, P., Trott, L.A., Brunskill, G.J., 1999. Mineralization of organic matter in intertidal sediments of a tropical semi-enclosed delta. *Estuar. Coast Shelf Sci.* 48, 451–467. <https://doi.org/10.1006/ecss.1998.0465>.
- Alongi, D.M., Wattayakorn, G., Boyle, S., Tirendi, F., Payn, C., Dixon, P., 2004. Influence of roots and climate on mineral and trace element storage and flux in tropical mangrove soils. *Biogeochemistry* 69, 105–123. <https://doi.org/10.1023/B: BIOG.0000031043.06245.af>.
- Alongi, D.M., Wattayakorn, G., Pfitzner, J., Tirendi, F., Zagorskis, I., Brunskill, G.J., Davidson, A., Clough, B.F., 2001. Organic carbon accumulation and metabolic pathways in sediments of mangrove forests in southern Thailand. *Mar. Geol.* 179, 85–103. [https://doi.org/10.1016/S0025-3227\(01\)00195-5](https://doi.org/10.1016/S0025-3227(01)00195-5).
- Anschutz, P., Dedieu, K., Desmazes, F., Chaillou, G., 2005. Speciation, oxidation state, and reactivity of particulate manganese in marine sediments. *Chem. Geol.* 218, 265–279. <https://doi.org/10.1016/j.chemgeo.2005.01.008>.
- Bally, G., Mesnage, V., Deloffre, J., Clarisse, O., Lafite, R., Dupont, J.P., 2004. Chemical characterization of porewaters in an intertidal mudflat of the Seine estuary: relationship to erosion-deposition cycles. *Mar. Pollut. Bull.* 49, 163–173. <https://doi.org/10.1016/j.marpolbul.2004.02.005>.
- Bava, K.A., Seralathan, P., 1999. Interstitial water and hydrochemistry of a mangrove forest and adjoining water system , south west coast of India. *Environ. Geol.* 38, 47–52.
- Beck, M., Dellwig, O., Liebbezeit, G., Schnetger, B., 2008. Spatial and seasonal variations of sulphate, dissolved organic carbon, and nutrients in deep pore waters of intertidal flat sediments. *Estuar. Coast Shelf Sci.* 79, 307–316. <https://doi.org/10.1016/j.ecss.2008.04.007>.
- Berner, R.A., 1980. *Early Diagenesis - A Theoretical Approach*. Princeton University Press, New Jersey.
- Berrêdo, J.F., Costa, M.L., da, Vilhena, M., do P.S.P., Santos, J.T. dos, 2008a. Mineralogia e geoquímica de sedimentos de manguezais da costa amazônica: o exemplo do estuário do rio Marapanim (Pará). *Rev. Bras. Geociências* 38, 24–35. <https://doi.org/10.25249/0375-7536.20083812435>.
- Berrêdo, J.F., Costa, M.L., da, Vilhena, M.S.P., Matos, C.R.L., 2016. Modificações nas propriedades físico-químicas de sedimentos de manguezais submetidos ao clima amazônico Changes in physicochemical properties of mangrove sediments under Amazonian climatic regime. *Bol. do Mus. Para. Emílio Goeldi Ciências Nat.* 11, 313–328.
- Berrêdo, J.F., Costa, M.L., Socorro, P., 2008b. Efeitos das variações sazonais do clima tropical úmido sobre as águas e sedimentos de manguezais do estuário do rio Marapanim , costa nordeste do Estado do Pará. *Acta Amazonica* 38, 473–482. <https://doi.org/10.1590/S0044-59672008000300012>.
- Bouillon, S., Middelburg, J.J., Dehairs, F., Borges, A.V., Abril, G., Flindt, M.R., Ulomi, S., Kristensen, E., 2007. Importance of intertidal sediment processes and porewater exchange on the water column biogeochemistry in a pristine mangrove creek (Ras Dege, Tanzania). *Biogeosciences* 4, 311–322. <https://doi.org/10.5194/bg-4-311-2007>.
- Breithaupt, J.L., Smoak, J.M., Smith III, T.J., Sanders, C.J., 2014. Temporal variability of carbon and nutrient burial, sediment accretion, and mass accumulation over the past century in a carbonate platform mangrove forest of the Florida Everglades.

- J. Geophys. Res. Biogeosci. 119, 2032–2048. <https://doi.org/10.1002/2014JG002715> (Received).
- Cline, J.D., 1969. Spectrophotometric determination OF hydrogen sulfide IN natural WATERS1. *Limnol. Oceanogr.* 14, 454–458. <https://doi.org/10.4319/lo.1969.14.3.0454>.
- Cohen, M.C.L., Behling, H., Lara, R.J., Smith, C.B., Matos, H.R.S., Vedel, V., 2009. Impact of sea-level and climatic changes on the Amazon coastal wetlands during the late Holocene. *Veg. Hist. Archaeobotany* 18, 425–439. <https://doi.org/10.1007/s00334-008-0208-0>.
- Cohen, M.C.L., Camargo, P.M.P., Pessenda, L.C.R., Lorente, F.L., De Souza, A.V., Corrêa, J.A.M., Bendassoli, J., Dietz, M., 2021. Effects of the middle Holocene high sea-level stand and climate on Amazonian mangroves. *J. Quat. Sci.* 36, 1013–1027. <https://doi.org/10.1002/jqs.3343>.
- Cohen, M.C.L., de Souza, A.V., Rossetti, D.F., Pessenda, L.C.R., França, M.C., 2018. Decadal-scale dynamics of an Amazonian mangrove caused by climate and sea level changes: inferences from spatial-temporal analysis and digital elevation models. *Earth Surf. Process. Landforms* 43, 2876–2888. <https://doi.org/10.1002/esp.4440>.
- Cohen, M.C.L., Lara, R.J., 2003. Temporal changes of mangrove vegetation boundaries in Amazonia: application of GIS and remote sensing techniques. *Wetl. Ecol. Manag.* 11, 223–231. <https://doi.org/10.1023/A:1025007331075>.
- Ding, S., Wang, Y., Wang, D., Li, Y.Y., Gong, M., Zhang, C., 2016. In situ , high-resolution evidence for iron-coupled mobilization of phosphorus in sediments. *Nat. Publ. Gr.* 1–11 <https://doi.org/10.1038/srep24341>.
- Dittmar, T., Hertkorn, N., Kattner, G., Lara, R.J., 2006. Mangroves, a major source of dissolved organic carbon to the oceans. *Global Biogeochem. Cycles* 20, 1–7. <https://doi.org/10.1029/2005GB002570>.
- Dittmar, T., Lara, R.J., 2001. Driving forces behind nutrient and organic matter dynamics in a mangrove tidal creek in North Brazil. *Estuar. Coast Shelf Sci.* 52, 249–259. <https://doi.org/10.1006/ecss.2000.0743>.
- Fossing, H., Jørgensen, B., 1989. Measurement of bacterial sulfate reduction in sediments: evaluation of a single-step chromium reduction method. *Biogeochemistry* 8, 205–222. <https://doi.org/10.1007/BF00002889>.
- Froelich, P.N., Klinkhammer, G.P., Bender, M.L., Luedtke, N.A., Heath, G.R., Cullen, D., Dauphin, P., Hammond, D., Hartman, B., Maynard, V., 1979. Early oxidation of organic matter in pelagic sediments of the eastern equatorial Atlantic: suboxic diagenesis. *Geochem. Cosmochim. Acta* 43, 1075–1090. [https://doi.org/10.1016/0016-7037\(79\)90095-4](https://doi.org/10.1016/0016-7037(79)90095-4).
- Gieskes, J.M., Gamo, T., Brumsack, H., 1991. Chemical methods for interstitial water analysis aboard JOIDES resolution, college station, Texas, ocean Drilling Program. *ODP Tech. Note* 15, 1–60. <https://doi.org/10.2973/odp.tn.15.1991>.
- Gleeson, J., Santos, I.R., Maher, D.T., Golsby-Smith, L., 2013. Groundwater-surface water exchange in a mangrove tidal creek: evidence from natural geochemical tracers and implications for nutrient budgets. *Mar. Chem.* 156, 27–37. <https://doi.org/10.1016/j.marchem.2013.02.001>.
- Glud, R.N., 2008. Oxygen dynamics of marine sediments. *Mar. Biol. Res.* 4, 243–289. <https://doi.org/10.1080/17451000801888726>.
- Gueiros, B.B., Machado, W., Filho, S.D.L., Lacerda, L.D., 2003. Manganese behavior at the sediment-water interface in a mangrove dominated area in Sepetiba Bay, SE Brazil. *J. Coast Res.* 19, 550–559.
- Hammer, Ø., Harper, D.A.T., Ryan, P.D., 2001. *Past : paleontological statistics software package for education and data analysis.* *Palaentol. Electron.* 4, 1–9.
- Hedges, J.L., Keil, R.G., Benner, R., 1997. What happens to terrestrial organic matter in the ocean. *Org. Geochem.* 27, 195–212.
- Holloway, C.J., Santos, I.R., Rose, A.L., 2018. Porewater inputs drive Fe redox cycling in the water column of a temperate mangrove wetland. *Estuar. Coast Shelf Sci.* 207, 259–268. <https://doi.org/10.1016/j.ecss.2018.04.016>.
- Holloway, C.J., Santos, I.R., Tait, D.R., Sanders, C.J., Rose, A.L., Schnetger, B., Brumsack, H.J., Macklin, P.A., Sippo, J.Z., Maher, D.T., 2016. Manganese and iron release from mangrove porewaters: a significant component of oceanic budgets? *Mar. Chem.* 184, 43–52. <https://doi.org/10.1016/j.marchem.2016.05.013>.
- Huerta-Diaz, A.-M., M, J.W., 1992. Pyritization of trace metals in anoxic marine sediments: RN - *Geochim. Cosmochim. Acta* 56, 2681–2702. *Geochim. Cosmochim. Acta* 56.
- Jennerjahn, T.C., Ittekkot, V., 2002. Relevance of mangroves for the production and deposition of organic matter along tropical continental margins. *Naturwissenschaften* 89, 23–30. <https://doi.org/10.1007/s00114-001-0283-x>.
- Kaiser, D., Kowalski, N., Böttcher, M.E., Yan, B., Unger, D., 2015. Benthic nutrient fluxes from mangrove sediments of an anthropogenically impacted estuary in Southern China. *J. Mar. Sci. Eng.* 3, 466–491. <https://doi.org/10.3390/jmse3020466>.
- Kauffman, J.B., Bernardino, A.F., Ferreira, T.O., Giovannoni, L.R., De Gomes, L.E.O., Romero, D.J., Jimenez, L.C.Z., Ruiz, F., 2018. Carbon stocks of mangroves and salt marshes of the Amazon region. Brazil. *Biol. Lett.* 14 <https://doi.org/10.1098/rsbl.2018.0208>.
- Kostka, J.E., Luther, G.W., 1994. Partitioning and speciation of solid phase iron in saltmarsh sediments. *Geochem. Cosmochim. Acta* 58, 1701–1710. [https://doi.org/10.1016/0016-7037\(94\)90531-2](https://doi.org/10.1016/0016-7037(94)90531-2).
- Kristensen, E., Bouillon, S., Dittmar, T., Marchand, C., 2008. Organic carbon dynamics in mangrove ecosystems : a review. *Aquat. Bot.* 89, 201–219. <https://doi.org/10.1016/j.aquabot.2007.12.005>.
- Kristensen, E., Connolly, R.M., Otero, X.L., Marchand, C., Ferreira, T.O., Rivera-Monroy, V.H., 2017. Biogeochemical cycles: global approaches and perspectives, mangrove ecosystems: a global biogeographic perspective: structure, function, and services. https://doi.org/10.1007/978-3-319-62206-4_6.
- Kristensen, E., King, G., Holmer, M., Banta, G., Jensen, M., Hansen, K., Bussarawit, N., 1994. Sulfate reduction, acetate turnover and carbon metabolism in sediments of the Ao Nam Bor mangrove, Phuket, Thailand. *Mar. Ecol. Prog. Ser.* 111, 245–255. <https://doi.org/10.3354/meps111245>.
- Kristensen, E., Mangion, P., Tang, M., Flindt, M.R., Holmer, M., Ulomi, S., 2011. Microbial carbon oxidation rates and pathways in sediments of two Tanzanian mangrove forests. *Biogeochemistry* 103, 143–158. <https://doi.org/10.1007/s10533-010-9453-2>.
- Lacerda Jr., L.D., M, G.R., Gueiros, B.B., 1999. *Manganese Dynamics in a Mangrove Mud Flat Tidal Creek in SE Brazil* 100, pp. 105–115.
- Lee, R.Y., Porubsky, W.P., Feller, I.C., McKee, K.L., Joye, S.B., 2008. Porewater biogeochemistry and soil metabolism in dwarf red mangrove habitats (Twin Cays, Belize). *Biogeochemistry* 87, 181–198. <https://doi.org/10.1007/s10533-008-9176-9>.
- Li, Y.-H., Gregory, S., 1974. Diffusion of ions in sea water and in deep-sea sediments. *Geochem. Cosmochim. Acta* 38, 703–714. [https://doi.org/10.1016/0016-7037\(74\)90145-8](https://doi.org/10.1016/0016-7037(74)90145-8).
- Liu, Y., Not, C., Jiao, J.J., Liang, W., Lu, M., 2019. Tidal induced dynamics and geochemical reactions of trace metals (Fe, Mn, and Sr) in the salinity transition zone of an intertidal aquifer. *Sci. Total Environ.* 664, 1133–1149. <https://doi.org/10.1016/j.scitotenv.2019.01.374>.
- Luther, G.W., Kostka, J.E., Church, T.M., Sulzberger, B., Stumm, W., 1992. Seasonal iron cycling in the salt-marsh sedimentary environment: the importance of ligand complexes with Fe(II) and Fe(III) in the dissolution of Fe(III) minerals and pyrite, respectively. *Mar. Chem.* 40, 81–103. [https://doi.org/10.1016/0304-4203\(92\)90049-G](https://doi.org/10.1016/0304-4203(92)90049-G).
- Marchand, C., Baltzer, F., Lallier-Vergès, E., Albéric, P., 2004. Pore-water chemistry in mangrove sediments: relationship with species composition and developmental stages (French Guiana). *Mar. Geol.* 208, 361–381. <https://doi.org/10.1016/j.margeo.2004.04.015>.
- Marchand, C., Lallier-Vergès, E., Allenbach, M., 2011. Redox conditions and heavy metals distribution in mangrove forests receiving effluents from shrimp farms (Teremba Bay, New Caledonia). *J. Soils Sediments* 11, 529–541. <https://doi.org/10.1007/s11368-010-0330-3>.
- Marchand, C., Lallier-Vergès, E., Baltzer, F., Albéric, P., Cossa, D., Baillif, P., 2006. Heavy metals distribution in mangrove sediments along the mobile coastline of French Guiana. *Mar. Chem.* 98, 1–17. <https://doi.org/10.1016/j.marchem.2005.06.001>.
- Matos, C.R.L., Berrêdo, J.F., Machado, W., Sanders, C.J., Metzger, E., Cohen, M.C.L., 2020. Carbon and nutrient accumulation in tropical mangrove creeks, Amazon region. *Mar. Geol.* 429 <https://doi.org/10.1016/j.margeo.2020.106317>.
- Matos, C.R.L., Mendoza, U., Diaz, R., Moreira, M., Belem, A.L., Metzger, E., Albuquerque, A.L.S., Machado, W., 2016. Nutrient regeneration susceptibility under contrasting sedimentary conditions from the Rio de Janeiro coast, Brazil. *Mar. Pollut. Bull.* 108 <https://doi.org/10.1016/j.marpolbul.2016.04.046>.
- Mcleod, E., Salm, R.V., 2006. *Managing Mangroves for Resilience to Climate Change* IUCN Global Marine Programme. Iucn.
- Meiggs, D., Taillefer, M., 2011. The effect of riverine discharge on biogeochemical processes in estuarine sediments. *Limnol. Oceanogr.* 56, 1797–1810. <https://doi.org/10.4319/lo.2011.56.5.1797>.
- Nascimento, W.R., Wal, P., Proisy, C., Lucas, R.M., 2013. Estuarine , Coastal and Shelf Science Mapping changes in the largest continuous Amazonian mangrove belt using object-based classification of multisensor satellite imagery. *Estuar. Coast Shelf Sci.* 117, 83–93. <https://doi.org/10.1016/j.ecss.2012.10.005>.
- Ogrinc, N., Fagnani, J., 2006. Phosphorus regeneration and burial in near-shore marine sediments (the Gulf of Trieste, northern Adriatic Sea). *Estuar. Coast Shelf Sci.* 67, 579–588. <https://doi.org/10.1016/j.ecss.2005.12.016>.
- Otero, X.L., Ferreira, T.O., Huerta-Díaz, M.A., Partiti, C.S.M., Souza, V., Vidal-Torrado, P., Macías, F., 2009. Geochemistry of iron and manganese in soils and sediments of a mangrove system, Island of Pai Matos (Cananea - SP, Brazil). *Geoderma* 148, 318–335. <https://doi.org/10.1016/j.geoderma.2008.10.016>.
- Otero, X.L., Ferreira, T.O., Vidal-Torrado, P., Macías, F., 2006. Spatial variation in pore water geochemistry in a mangrove system (Pai Matos island , Cananea-Brazil). *Appl. Geochem.* 21, 2171–2186. <https://doi.org/10.1016/j.apgeochem.2006.07.012>.
- Otero, X.L., Macías, F., 2003. Spatial variation in pyritization of trace metals in salt-marsh soils. *Biogeochemistry* 62, 59–86. <https://doi.org/10.1023/A:1021115211165>.
- Ovalle, A.R.C., Rezende, C.E., Lacerda, L.D., Silva, C.A.R., 1990. Factors affecting the hydrochemistry of a mangrove tidal creek, sepetiba bay, Brazil. *Estuar. Coast Shelf Sci.* 31, 639–650. [https://doi.org/10.1016/0272-7714\(90\)90017-L](https://doi.org/10.1016/0272-7714(90)90017-L).
- Pan, F., Guo, Z., Cai, Y., Fu, Y., Wu, J., Wang, B., Liu, H., Gao, A., 2020. Cyclical patterns and (im)mobilization mechanisms of phosphorus in sediments from a small creek estuary: evidence from in situ monthly sampling and indoor experiments. *Water Res.* 171, 115479. <https://doi.org/10.1016/j.watres.2020.115479>.
- Pan, F., Liu, H., Guo, Z., Cai, Y., Fu, Y., Wu, J., Wang, B., 2019a. Metal/metalloid and phosphorus characteristics in porewater associated with manganese geochemistry : a case study in the Jitulong River Estuary, China. *Environ. Pollut.* 255, 113134. <https://doi.org/10.1016/j.envpol.2019.113134>.
- Pan, F., Liu, H., Guo, Z., Li, Z., Wang, B., Cai, Y., Gao, A., 2019b. Effects of tide and season changes on the iron-sulfur-phosphorus biogeochemistry in sediment porewater of a mangrove coast. *J. Hydrol.* 568, 686–702. <https://doi.org/10.1016/j.jhydrol.2018.11.002>.
- Pratihary, A., Naik, R., Karapurkar, S., Gauthankar, M., Khandeparker, R., Manjrekar, S., Gauns, M., 2021. Benthic exchange along a tropical estuarine salinity gradient during dry season: biogeochemical and ecological implications. *J. Sea Res.* 177, 102124. <https://doi.org/10.1016/j.seares.2021.102124>.
- Raiswell, R., Canfield, D.E., 1998. Sources of iron for pyrite formation in marine sediments. *Am. J. Sci.* 298, 219–245. <https://doi.org/10.2475/ajs.298.3.219>.

- Ranjan, R.L., Routh, J., Ramanathan, A.L., Klump, J.V., 2011. Elemental and stable isotope records of organic matter input and its fate in the Pichavaram mangrove – estuarine sediments (Tamil Nadu, India). *Mar. Chem.* 126, 163–172. <https://doi.org/10.1016/j.marchem.2011.05.005>.
- Rao, K., Priya, N., Ramanathan, A.L., 2018. Impact of seasonality on the nutrient concentrations in Gautami-Godavari estuarine mangrove complex, Andhra Pradesh, India. *Mar. Pollut. Bull.* 129, 329–335. <https://doi.org/10.1016/j.marpolbul.2018.02.052>.
- Redfield, A.C., Ketchum, B.H., Richards, A., 1963. The influence of organisms on the composition of sea water. In: Hill, M.M. (Ed.), *The Sea*. Interscience, Geneva, pp. 26–77.
- Rozan, T.F., Taillefert, M., Trouwborst, R.E., Glazer, B.T., Ma, S., Herszage, J., Valdes, L.M., Price, K.S., Luther, G.W., 2002. Iron-sulfur-phosphorus cycling in the sediments of a shallow coastal bay: implications for sediment nutrient release and benthic macroalgal blooms. *Limnol. Oceanogr.* 47, 1346–1354. <https://doi.org/10.4319/lo.2002.47.5.1346>.
- Rusch, A., Huettel, M., Wild, C., Reimers, C.E., 2006. Benthic oxygen consumption and organic matter turnover in organic-poor, permeable shelf sands. *Aquat. Geochem.* 12, 1–19. <https://doi.org/10.1007/s10498-005-0784-x>.
- Sadat-Noori, M., Glamore, W., 2019. Porewater exchange drives trace metal, dissolved organic carbon and total dissolved nitrogen export from a temperate mangrove wetland. *J. Environ. Manag.* 248, 109264. <https://doi.org/10.1016/j.jenvman.2019.109264>.
- Sanders, C.J., Eyre, B.D., Santos, I.R., Machado, W., Luiz-silva, W., Smoak, J.M., Breithaupt, J.L., Ketterer, M.E., Sanders, L., Marotta, H., Silva-filho, E., Al, S.E.T., 2014. Impacted mangrove wetland. *Geophys. Res. Lett.* 2475–2480. <https://doi.org/10.1002/2014GL059789> (Received).
- Sanders, C.J., Santos, I.R., Maher, D.T., Sadat-Noori, M., Schnetger, B., Brumsack, H.J., 2015. Dissolved iron exports from an estuary surrounded by coastal wetlands: can small estuaries be a significant source of Fe to the ocean? *Mar. Chem.* 176, 75–82. <https://doi.org/10.1016/j.marchem.2015.07.009>.
- Santos-Echeandia, J., Prego, R., Cobelo-García, A., Millward, G.E., 2009. Porewater geochemistry in a Galician Ria (NW Iberian Peninsula): implications for benthic fluxes of dissolved trace elements (Co, Cu, Ni, Pb, V, Zn). *Mar. Chem.* 117, 77–87. <https://doi.org/10.1016/j.marchem.2009.05.001>.
- Seeberg-Elverfeldt, J., Schlüter, M., Feseker, T., Kölling, M., 2005. Rhizon sampling of porewaters near the sediment-water interface of aquatic systems. *Limnol. Oceanogr. Methods* 3, 361–371. <https://doi.org/10.4319/lom.2005.3.361>.
- Sherman, R.E., Fahey, T.J., Howarth, R.W., 1998. Soil-plant interactions in a neotropical mangrove forest: iron, phosphorus and sulfur dynamics. *Oecologia*. <https://doi.org/10.1007/s004420050553>.
- da Silva, C.A., Souza-Filho, P.W.M., Rodrigues, S.W.P., 2009. Morphology and modern sedimentary deposits of the macrotidal Marapanim Estuary (Amazon, Brazil). *Continent. Shelf Res.* 29, 619–631. <https://doi.org/10.1016/j.csr.2008.09.018>.
- Taillardat, P., Ziegler, A.D., Friess, D.A., Widory, D., David, F., Ohte, N., Nakamura, T., Evaristo, J., Thanh-Nho, N., Van Vinh, T., Marchand, C., 2019. Assessing nutrient dynamics in mangrove porewater and adjacent tidal creek using nitrate dual-stable isotopes: a new approach to challenge the Outwelling Hypothesis? *Mar. Chem.* 214, 103662. <https://doi.org/10.1016/j.marchem.2019.103662>.
- Tait, D.R., Maher, D.T., Sanders, C.J., Santos, I.R., 2017. Radium-derived porewater exchange and dissolved N and P fluxes in mangroves. *Geochem. Cosmochim. Acta* 200, 295–309. <https://doi.org/10.1016/j.gca.2016.12.024>.
- Terada, K., Koibuchi, Y., Isobe, M., 2017. Rainfall effect on sediment and nutrient fluxes in a small mangrove river, Okinawa, Japan. *J. Mar. Res.* 75, 1–17. <https://doi.org/10.1357/002224017821219027>.
- Thanh-Nho, N., Marchand, C., Strady, E., Van Vinh, T., Taillardat, P., Cong-Hau, N., Nhu-Trang, T.T., 2020. Trace metal dynamics in a tropical mangrove tidal creek: influence of porewater seepage (Can Gio, Vietnam). *Front. Environ. Sci.* 8 <https://doi.org/10.3389/fenvs.2020.00139>.
- Thanh-Nho, N., Marchand, C., Strady, E., Vinh, T. Van, Nhu-Trang, T.T., 2019. Metals geochemistry and ecological risk assessment in a tropical mangrove (Can Gio, Vietnam). *Chemosphere* 219, 365–382. <https://doi.org/10.1016/j.chemosphere.2018.11.163>.
- Thibault de Chanvalon, A., Metzger, E., Mouret, A., Knoery, J., Geslin, E., Meysman, F.J.R., 2017. Two dimensional mapping of iron release in marine sediments at submillimetre scale. *Mar. Chem.* 191, 34–49. <https://doi.org/10.1016/j.marchem.2016.04.003>.
- Vilhena, M.D.P.S.P., Costa, M.L. Da, Berrêdo, J.F., 2010. Continental and marine contributions to formation of mangrove sediments in an Eastern Amazonian mudplain: the case of the Marapanim Estuary. *J. South Am. Earth Sci.* 29, 427–438. <https://doi.org/10.1016/j.jsames.2009.07.005>.
- Wang, W.W., Li, D.J., Zhou, J.L., Gao, L., 2011. Nutrient dynamics in pore water of tidal marshes near the Yangtze Estuary and Hangzhou Bay, China. *Environ. Earth Sci.* 63, 1067–1077. <https://doi.org/10.1007/s12665-010-0782-1>.
- Weston, N.B., Porubsky, W.P., Samarkin, V.A., Erickson, M., Macavoy, S.E., Joye, S.B., 2006. Porewater stoichiometry of terminal metabolic products, sulfate, and dissolved organic carbon and nitrogen in estuarine intertidal creek-bank sediments. *Biogeochemistry* 77, 375–408. <https://doi.org/10.1007/s10533-005-1640-1>.
- Wu, Z., Zhou, H., Ren, D., Gao, H., Li, J., 2015. Processes controlling the seasonal and spatial variations in sulfate profiles in the pore water of the sediments surrounding Qi'ao Island, Pearl River Estuary, Southern China. *Continent. Shelf Res.* 98, 26–35. <https://doi.org/10.1016/j.csr.2015.02.001>.
- Yasui, S., Kanda, J., Usui, T., Ogawa, H., 2016. Seasonal variations of dissolved organic matter and nutrients in sediment pore water in the inner part of Tokyo Bay. *J. Oceanogr.* 72, 851–866. <https://doi.org/10.1007/s10872-016-0382-0>.